Mathematical Modelling of Engineering Problems
Vol. 12, No. 5, May, 2025, pp. 1718-1730
Journal homepage: http://iieta.org/journals/mmep

A Comparison Analysis of Design and Performance Optimization of Gas Turbine Combustor for Better Combustion Efficiency

Mohit Bansal*, Abdur Rahim

Department of Mechanical Engineering, Jamia Millia Islamia, New Delhi 110025, India

Corresponding Author Email: bansalmohit01@gmail.com

https://doi.org/10.18280/mmep.120527

Received: 7 February 2025
Revised: 16 April 2025
Accepted: 22 April 2025
Available online: 31 May 2025

Keywords:
gas turbine combustor, combustion process, fuels, combustion shape, swirler effect, velocity

ABSTRACT

Combustion in a typical open cycle gas turbine is a continuous process in which fuel burns in the air provided by the compressor. This research analyses the gas turbine combustor using various kinds of fuel types, temperatures, combustor shapes, and swirl effects. The performance of gas turbine combustors is meticulously scrutinized in a comprehensive analysis that encompasses an array of different fuel types including methane, hydrogen, syngas, biogas, and propane. Furthermore, the evaluation extends to examining the gas turbine under a diverse range of temperature conditions to provide a holistic view of its operational efficiency. In addition to fuel variations and temperature influences, the study delves into the impact of different combustor shapes on the overall performance of the gas turbine combustor. This detailed investigation aims to unravel the intricate interactions between combustor design and fuel composition to enhance the turbine's efficiency and reliability. Finally, the assessment is rounded off by considering the effects of incorporating a swirler into the combustor setup. Through this exhaustive analysis, a deeper understanding of the factors influencing gas turbine combustor performance is gained. The gas turbine's optimal combustion process is achieved with a can type combustion with methane fuel and an inlet temperature of 1700 K and a 30° swirler angle. Various fuels, temperature, combustion shape and swirled effect are analyzed for different gas turbine combustor model which demonstrate low emissivity, low fuel cost and poor time consumption to effectively improve the combustion performance.

1. INTRODUCTION

In today's competitive business environment, lowering operating and maintenance costs while raising productivity is one strategy to boost the profitability of machinery, equipment, or a processing plant. Reliability and availability are the two most sought-after characteristics in aircraft and industrial applications, where Gas Turbines (GT) are among the priciest devices. Trillions of dollars have been invested worldwide in the upkeep and operation of GT during the last few decades [1]. In order to reduce CO_2 emissions globally in the future, gas turbine technology is crucial. At the moment, CO_2 reduction is the driving force in the electricity generation sector, which contributes the most to CO_2 emissions [2]. Nowadays, gas turbines are employed in many different applications, ranging from large-scale power generation to jet engines. Certain gas turbine applications are finding it difficult to use new materials that are intended for strength rather than corrosion resistance. Numerous research on dynamic performance analysis based on operating conditions and steady-state performance analysis have been conducted [3]. The gas turbine compressor in particular has a relatively limited operating window. In order to lower NOx emissions, lean-premixed turbulent combustion is made easier with the help of the combustor. Lean-premixed turbulent combustion has minimal emission characteristics, however because of pressure dynamics, the flame is highly unstable. Turbines from the preceding generation with less horsepower have been used to power crude oil pumps and vapour recovery compressors when electricity is not available. There are three sections to the can combustor's airflow. The dome, or front end of the combustor, is where the initial portion of the airflow passes. This portion of the air is combined with fuel that is injected by the nozzles to cool the dome. The study's focus was on the second and third airflow segments that pass through the inner and outer annulus. In order to simulate the geometry of the combustor and use kinetic and turbulence models for combustion stability and flame stabilization, research have been carried out to examine combustor phenomena [4].

Traditionally employed simple-cycle gas turbines for the generation of limited peak electricity. Moreover, industrial facilities generate power on-site using gas turbine units, typically in conjunction with the production of process heat, such as process steam and hot water [5]. In combustor the swirler vane was placed in front of the combustor. The swirler vanes allowed equal amounts of air to enter. The fuel nozzles are located directly behind the swirler vane and are uniformly placed around the casting perimeter. The dome, primary, secondary, and dilution holes were the four zones that made up the combustor. A constant hollow casting creates a

homogeneous fluid flow. In both the main and dome zones, the fuel and air were blended uniformly. In comparison to the secondary zone, the primary zone attained the maximum flame temperature [6]. Increased use of gas turbines for base load applications has also been made possible by improved fuel resource availability, such as natural gas, sharply lower capital costs, and the development of advanced cycles. Nevertheless, when the most accessible technological advancements were utilized, the rate of progress slowed down. Furthermore, because scale economies have negative effects, it is usually more economical to design a smaller power plant for small-scale power output (less than 50 MWe). This power output range's combined cycle facilities are trustworthy and long-lasting, while frequently having greater upfront expenditures and lower electrical effectiveness [7]. At a fair price, gas turbine-based power plants' efficiency could be increased by thermodynamic cycle improvements including recovery, among- or after-cooling, and cycle integration (e.g., Mixed Air Steam Turbines, or MAST). There isn't any fuel-flexible equipment on the market that can process natural gas and hydrogen together in the whole range of 0–100% [8].

A comprehensive statistical analysis of combustor performance using different fuels has been made possible by examining the impact of fuel composition and attributes on sooty flame propensity and lean blowout (LBO). However, not all aromatics emit the same amount of smoke and pollutants. Examining a Rich/Quench/Lean (RQL) can combustor performs during combustion while using combined natural gas and hydrogen fuel. For a variety of hydrogen volumetric percentages, CFD numerical simulations have actually been carried out with a 10% step and adding ranging from 0% to 90%. Nevertheless, the turbine blades' thermal resistance might not be met by the outlet temperature distribution [9]. Two-stage gas turbine converters, both with and without slot film cooling operating at 0.25 MPa, are utilized to study flame stability and emissions control during liquid ammonia spray combustion, with an input thermal power of up to 230 kW. The trials were carried out in a small test station for a gas turbine combustor, which was designed to burn gaseous ammonia initially. The combustor's NO emissions still need to be further decreased, even though the N_2O emissions were manageably low. The effects of various fuel-air equivalent ratios and chamber pressures on turbulence ignition and swirling injection are investigated by large-scale eddy simulations in a dual-swirl gas turbine model combustor. Numerical results demonstrate the complex interaction between high-pressure turbulent flame and spinning flows. Prior research has documented difficulties in the combustion of ammonia. The low burning velocity of ammonia-air mixes is approximately five times lower than that of methane-air mixtures under stoichiometric circumstances. NTP stated that low ammonia-air mixture burning velocities were required because they prevented effective turbulent mixing and necessitated a long enough fluid residence time in their gas turbine combustor. The enhanced combustor's exit temperatures drop and exhibit a more uniform distribution as a result of coupled film cooling, which lowers the pattern factor. Moreover, because of its substantial thrust, good efficiency, and comparatively low combustor emissions [10].

This section effectively provides a comprehensive overview of gas turbine combustors and highlights their significance in industrial and power generation applications. The insights gained from this study have the potential to support the development of next-generation low-emission combustors, which will be essential in future applications that demand both high performance and environmental sustainability. These advancements can contribute significantly to improving gas turbine efficiency and reliability, while also aligning with global efforts to reduce carbon emissions in the energy sector. So, Gas turbine combustor is analysed by considering various conditions such as different fuels, combustor shapes, swirl effects and temperatures which are clearly discussed in the following literature review section.

2. LITERATURE REVIEW

Study of gas turbine performance with varying design and process conditions such as different kinds of fuels, combustor shapes, varying swirls, and different temperatures Papers were collected from 2016 to 2023. The study analyzed 25 references related to the varying swirl, different temperatures, combustor shapes, and kinds of fuels for gas turbine combustor.

2.1 Different kind of fuels for gas turbine combustor

Fuel is mixed with the air stream via a row of vanes. A swirl stabilized flame develops behind a bluff body on the combustor's centerline after the fuel-air mixture enters the combustor. After passing through a primary fuel injector, the main stage air travels along the rear of the combustion liner. The research publications on gas turbine combustion various fuels that have been reviewed are listed below.

Table 1. Properties of hydrogen fuels

Properties	Hydrogen
Formula	H_2
Flammability limits (vol %)	4-75
Ignition energy (MJ)	0.018
Flame speed (cm/s)	250
Lower calorific value (MJ/kg)	120
Stoichiometric fuel concentration (%)	29.6
Molecular weight(kg/kmol)	2
Volumetric energy density (MJ/L)	8.4
Density (kg/m^3)	0.08
Auto ignition temperature (°C)	500-571
Stoichiometric air/fuel ratio	34.3
Adiabatic flame temperature (K)	2525

Kahraman et al. [11] suggested a hydrogen-powered gas turbine engine's tubular combustion chamber feasibility of using hydrogen as a substitute fuel. Gaseous hydrogen combustion properties in a combustor of a Rolls-Royce Nene turbojet engine have been studied computationally at thermal power levels and different excess air ratios (EAR).

Numerical simulations have been conducted to analyze temperature distributions, combustion efficiency, pressure drops, and velocity changes within the combustion chamber of a gas turbine. The investigations were carried out at thermal power levels corresponding to engine speeds of 10000 rpm (1480 kW), 11000 rpm (2290 kW), and 12000 rpm (2980 kW).

But as additional air enters the combustion chamber, its temperature drops. The numerical analyses were conducted using hydrogen fuels. The characteristics of hydrogen fuels are listed in Table 1.

For the combustor modeling, the following physical values were used: The combustor has a 145 mm for the maximum radius, 90 mm for the combustor's inlet and outflow,

dimensions are 620 mm in length with 35 mm for the primary air intake where RC_{in} equals RC_{out} . Installed on a symmetrical axis, the fuel inlet has a radius of R_f = 2 mm. Eqs. (1) and (2) describe the reaction mechanisms involving the ratio of hydrogen to excess air.

$$H_2 + EAR.\frac{1}{2}(O_2 + 3{,}76N_2) \rightarrow H_2O + (EAR - 1).\frac{1}{2}O_2 + EAR.\frac{3{,}76}{2}N_2 \quad (1)$$

$$EAR = \frac{\left(A/F\right)_a}{\left(A/F\right)_s} \quad (2)$$

The stoichiometric air-fuel ratio is denoted by $\left(A/F\right)_s$ while the actual air-fuel ratio at the combustion chamber inlet is represented by $\left(A/F\right)_a$.

Liu et al. [12] analysed the effects of pilot split, fuel injector positions, and fuel types on combustion efficiency in a DLE combustor meant for a micro-gas turbine. A thorough investigation was conducted to ascertain whether using raw biogas in low NOx combustion for micro gas turbines was feasible. The operating conditions of the engine in an air-conditioned environment were analyzed, along with investigating the lean ignition and extinction characteristics across different fuel compositions. The findings showed that reducing both fuel Wobbe Index (WI) and NOx emissions jointly had a noticeable benefit. The combustor demonstrates favorable combustion characteristics with low pollutant emissions across engine loads from 50% to 100%, given that the fuel air-to-fuel ratio is maintained above the required threshold. The NOx emission has the lowest value and has a significant impact on NOx emissions for a particular sample division. Nevertheless, a number of obstacles prevent biogas from being used in micro gas turbines. Tables 2 and 3 display the various fuel inlet combination options. The fuel compositions and their WI are listed, and the impact of various fuel mixing patterns on combustion performance is analyzed.

Wang et al. [13] suggested the impact of effusion cooling in a combustion chamber liner. Several cooling holes inclination angles were taken into consideration. Propane was utilized as fuel in numerical simulations based on a Can-type gas turbine compressor. Fuels made of propane are thought to be the most basic hydrocarbons, and they burn similarly to fuels made of more complicated hydrocarbons. There are eighteen 45-degree swirler vanes on the combustor. On the 90° cone surface, there are ten 1.7 mm-diameter holes from which fuel is injected. There are two rows of holes in the chamber's liner, each with a diameter of 10 mm. The first row has six dilution holes, and the second row has twelve dilution holes.

Table 2. Compositions of the fuels

Fuel	WI/MJ (m^3)	LHV/MJ (m^3)	CH_4 (vol.%)	Molar Mass (kg/kmol)	CO_2 (vol.%)	Density (kg/m^3)
F1	17.57	17.85	50	30	50	1.3465
F2	21	21.063	59	27.48	41	1.23301
F3	23.5	22.3839	62.7	26.444	37.3	1.186353
F4	26	24.276	68	24.96	32	1.11952
F5	43.21	33.6294	94.2	17.624	5.8	0.789138

Table 3. Combinations of different fuel intakes

Parameter	Combinations				
	C1	C2	C3	C4	C5
Fuel intakes	1+4	1+2+3	1+3	1+2	1+2+3

Separate streams of fuel and oxidizer enter a reaction zone. The mixture fraction is the only parameter that can be used to describe the thermochemistry of combustion under specific assumptions. By eliminating issues with enclosed nonlinear mean reaction rates, combustion decreases to a mixing problem. Eq. (3) presents the transport equation for this mixture percent movement.

$$\frac{\partial \bar{\rho}\tilde{f}}{\partial t} + \frac{\partial \bar{\rho}\tilde{f}\tilde{u}_j}{\partial x_j} = + \frac{\partial}{\partial x_j}\left(\Gamma_f \frac{\partial \tilde{f}}{dx_j}\right) \quad (3)$$

where, t is the time, and $\bar{\rho}$ is the gas mixture's time-averaged density. While x_j represents the direction's spatial Cartesian coordinate, the Cartesian component of velocity's Favre's average is represented by $\tilde{u}_j$. This quantity's turbulent diffusivity is represented by Γ_f, while the mixture fraction's Favre's average is symbolized by $\tilde{f}$. In the Table 4, the comparison of equal molar syngas and H_2 rich syngas, is given.

Table 4. Comparison of equal molar syngas and H_2 rich syngas

Composition	Flow Rate of Fuel (480 kW)	Heat Input ($\dot{m}_f$=0.0096 kg/s)
Equal molar	0.0274 kg/s	273 kW
H_2-rich	0.0138 kg/s	364 kW

Ajvad and Shih [14] suggested a numerical investigation on how an inventive micro gas turbine's casing rotation affects the fuel's ability to burn H_2/CO syngas. The computational model is composed of a three-dimensional realizable turbulent flow model that is compressible and k-ε. It also includes an assumed PDF for the combustion procedure, which builds an assumed unidirectional flamelet. The can-type combustor measures 220 mm in length, with the combustor itself and its casing having dimensions of 75 and 95 mm. The air inlet holes surrounding the combustor aim to accomplish the following objectives: maintaining maximum flame temperature in the initial stage, ensuring minimal flow disturbance in the next phase, and effectively mixing in the dilution region. The external swirling flow around the combustor reduces the flame size and enhances mixing, although the exact influence on combustion remains uncertain.

The mixing fraction (*f*) is represented as in Eq. (4).

$$f = \frac{Z_i - Z_{ox}}{Z_{i,fuel} - Z_{i,ox}} \quad (4)$$

where, Z_i is the mass fraction of a certain element i. The values at the oxidizer stream inlet and the fuel stream inlet are indicated by the subscripts fuel and ox, respectively. These flames can be characterized using specified variables: f and X.

$$X = 2D|\nabla f|^2 \quad (5)$$

where, the diffusion coefficient represented by D is used.

Chen et al. [15] suggested the stability of methane-air mixtures on platinum and their combustion properties in catalytic micro-combustors. In order to provide recommendations for the ideal design of combustor dimensions, the study examined how variations in gap size, wall thickness, and combustor length affect combustion stability and overall combustor performance. The combustor is made up of two parallel plates that are 8.0 mm long, 0.2 mm thick, and infinitely wide. There is a 0.8 mm gap between them. These numbers indicate the "nominal" dimensions of the combustor. However, this trend is reversed at lower inlet flow velocities.

Bonasio and Ravelli [16] examine the viability of directly using ammonium in a micro gas turbine (MGT) from a thermodynamic perspective. To simulate the behavior of a 100 kW MGT working at both full and partial load, a modeling technique was developed. In order to predict fluctuations in electric, thermal, and overall efficiency along with the composition of exhaust gas throughout a load range spanning from 40% to 100%, combustor validation was subjected to increasing amounts of ammonia fed with natural gas as fuel.

It was shown that switching from natural gas (NG) to ammonia decreased electrical efficiency by roughly 0.5 percentage points (pp), regardless of power output; however, as a result, exhaust gas heat recovery rose. To benefit from zero CO_2 emissions, compressor-turbine matching needs to be adjusted to account for the drop in fuel calorific value. However, Practical combustion produces comparatively high NOx emissions.

2.2 Varying temperature for gas turbine combustor

One important consideration in this regard is the temperature of the combustor wall. Heat loss to the confinement and its effect on flame stability have drawn increased attention in the last few years. A gas turbine model combustor's wall temperatures vary from several hundred to over two thousand Kelvin. Some research articles on various temperatures for gas turbine combustion models are examined below.

Singh et al. [17] suggested low temperature combustion regimes include reactivity regulated compression ignition (RCCI), premixed charge compression ignition (PCCI), and compression ignition (CI). These are used for comparing emission measurements and engine performance. For all combustion modes, the coolant, fuel, and lubricating oil were maintained at 90℃, 25℃, and 60℃, correspondingly. Probabilistic analyses were performed between the crucial parameters of the baseline CI, PCCI, and RCCI combustion modes at both low and high engine loads. The results showed improved engine performance as well as the low temperature combustion (LTC) mode's emission characteristics, particularly for the RCCI mode's combustion.

A gas turbine outfitted with modern, cutting-edge components is used. Figure 1 shows the modular arrangement, the constant essential performance attributes for the design investigations.

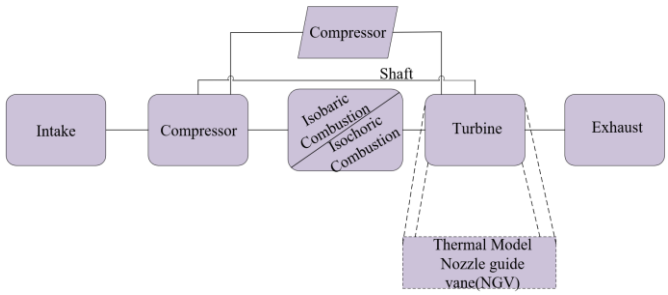

Figure 1. Schematic view of the gas turbine model

Schulz and Noiray [18] examined the second stage of air combustion at high pressure in a sequential combustor. The mixing temperature, pressure and species composition at the domain's inlet are the necessary input parameters. Initially, 0-D and 1-D simulations yield combustion regime maps that demonstrate the coexistence of flame propagation, flame propagation assisted by auto ignition, and flame propagation via auto ignition. When coupled with semi-detailed chemistry in three-dimensional large eddy simulations (LES), these regime globes provide an understanding of the combustion modes that arise in turbulent sequential combustors. In these simulations, methane and vitiated gas mixes were used at temperatures between 1000 and 1600 K. It using an input mixture, a 1-D transient flame simulation was performed at 1400 K. The modeling of steady-state combustion operating circumstances incorporates a transient shift in the input temperature that modifies the combustion regime. The flame might spread against the incoming flow following the auto ignition event.

Somarathne et al. [19] explored temperature and OH content's impact on turbulent, non-premixed air swirl/ammonia (NH_3)/methane (CH_4) flames' NO emission properties in two-stage high-pressure regions combustors. The energy percentage of NH_3 (E_{NH3}) in mixes of CH_4 and NH_3 was used to generate emission information from model fires using large-eddy simulations and a finite-rate chemistry approach. The combustor measured 150 mm in height and 72 mm in inner diameter (D). The combustor's bluff body functioned as the flame stabilizing surface, while the outer and inner swirlers had swirl numbers of 0.68 and 0.69, respectively, due to their 40° vane angles. The temperature of the fuel was 300 K, while the input air was 500 K. There was 0.5 MPa of combustor pressure. But the middle plane's xNO was not standardized at 16% O_2.

NH_3 mostly replaced CH_4 in the energy component of NH_3 in the CH_4/NH_3 blends, E_{NH3}, by accounting for the LHV of both fuels. Eq. (6) provides a quick summary of the relationship between E_{NH3} and the mole percent of NH_3 in a CH_4/NH_3 fuel combination, or XNH_3.

$$E_{NH3}\% = \frac{X_{NH3} \times LHV_{NH3} \times 100}{X_{NH3} \times LHV_{NH3} + (1 - X_{NH3}) \times LHV_{CH4}} \quad (6)$$

The NO-temperature data at E_{NH3} of 10% to 60% as the temperature rose above 2100 K, the exponential increase in NO content was in line with the thermal NO seen in CH_4/air fires. Nevertheless, the maximum permissible NO level for CH_4/air fires was only set at about 2000 ppm, which was far lower than the norms for these circumstances. These effects may be responsible for the almost 30% decrease in NO levels at E_{NH3}. All things considered, these results demonstrate that the flame temperature had a considerable impact on the OH

concentration, which in turn managed the CH_4/NH_3/air flames' NO levels.

Nau et al. [20] analysed the measurements of the wall temperature in gas turbines and gas turbine model combustors can be made using phosphor thermometry. On a ceramic surface, accomplishments up to 1700 K in measures are demonstrated with good accuracy. The temperatures on the quartz walls of the combustor were also recorded with the same equipment, and these readings can be utilized as simulation boundary conditions. Either the Nd: YAG laser the high-speed dye laser was used to excite the phosphor samples and either a spectrometer, high-speed camera, or photomultiplier tube (PMT) was used to find the phosphorescence signals. At lengthy degradation inflation, it is unlikely that the transitory fluorescence will have a substantial impact on the decomposition measurements.

The air excess ratio (λ) of the flame was varied between 1.9 and 3.1 to change the temperature on the probe. The stoichiometry was gradually adjusted to λ = 2.55 from a starting point of λ = 2.2, then lowered to 1.8 and then raised to 3.1 once more. The TBC-covered wall of a gas turbine combustor was replicated using a coated ceramic probe. With extreme precision and accuracy, temperatures as high as 1700 K were recorded.

Mekhrengin et al. [21] indicated that the development of a spectrum approach has made it possible to detect the temperature of the gas flow inside the combustion chamber. The gas turbine engine combustion chamber's hottest zones have temperatures that vary from 600 to 2200. Plank's law yields Wien's displacement law, which describes black body radiation for the given temperatures. Experiments conducted on the gas turbine engine in the field verified that the system under presentation is capable of monitoring temperatures between 810 to 1120°C with a 3% measurement error. On the other hand, the system's response time for the flame stability measurement needs to be enhanced. Eq. (7) provides a governing formula for determining the temperature inside the combustion chamber.

$$\ln(\lambda^5 I) - \ln(\varepsilon C_1) = -\frac{c_2}{\lambda T} \quad (7)$$

Eq. (7) depicts a straight line in coordinates $x = {C_2}/{\lambda}$ and $y = \ln(\lambda^5 I)$, which are known as the Wien's coordinates, where $\varepsilon = const$. Hence, without accounting for an emission coefficient, the soot temperature is inversely proportional to the angle of the line in these coordinates.

Chen et al. [22] examined how the effects of fuel variation and input air temperature on the features of combustion stability were observed in a gas turbine simulation combustor. As fuels, three distinct single-component hydrocarbons were employed: the linear alkane n-decane, the cyclic alkane, and the branched alkane iso-octane. The air entering the system had a temperature range of 383 to 483 K. The experiments used a consistent equivalence ratio of 0.86. Despite this uniformity, the flames of methyl cyclohexane (MCH) and iso-octane exhibited markedly different behaviors, consistently displaying unstable combustion from a thermo-acoustic standpoint across all examined conditions. Furthermore, an identifiable mode-shift phenomena was seen upon raising the input air's temperature from 403 K to 423 K. However, accurately determining the velocity distribution is difficult when dealing with liquid phases at low inlet air temperatures.

2.3 Different shapes of gas turbine combustor

A gas turbine is an internal combustion engine that converts the chemical energy of fuel into mechanical power. There are three primary parts to it: the turbine, combustor, and compressor. A can-type combustor, which had a single chamber, was employed in early gas turbine engines. There are currently three primary configurations: can, annular, and cannular. Few research articles explaining various shapes of gas turbine combustor was reviewed below.

Zettervall et al. [23] utilized both computational and experimental techniques, the NTNU's full annular model gas turbine combustor, which runs on both methane- and ethylene-air mixes, exhibits unstable gas turbine combustion. The entire annular combustor, situated in a sizable outside space, along with the eighteen input tubes and swirlers make up the computational setup. To create a shared plenum, 18 premixed flames with dimensions ranging of D_a = 170 mm are arranged in a circular. Each burner is designed with a conical bluff-body at its center (with a diameter of 13.0 mm) and surrounded by a cylindrical tube (with a length of 150 mm and a diameter of 18.9 mm). Top of FormBottom of Form a six-vane swirler positioned 10 mm before the flow alters its direction counter clockwise when observed from above (downstream). The inner and outer lengths of the quartz tubes that were utilized to form the elongated cage around the 18 flames were different, measuring L_I =130 and L_O =300 mm, respectively. The enclosure's measurements between the inner and outer tubes were D_I= 127 mm and D_0 = 212 mm.

A compressible chemistry with a finite rate makes up the computational model. The combustion chemistry of ethylene and methane in a large eddy simulation model in skeletal terms. The C_2H_4-air and CH_4-air conditions behave quite differently, according to experiments and LESs; the difference in such causes the nearby flames in the C_2H_4-air conditions to interact uniquely, resulting in significantly smaller flames than in the CH_4-air conditions. The two counter-rotating modes that make up the combustion dynamics of the CH_4-case are two modes: there is a noticeable longitudinal mode at 924 Hz and a faint azimuthal mode at 1698 Hz. In essence, these modes neutralize one another. Preliminary experimental data also support this difference in modal behaviour.

Table 5. Experimental text and the numerical simulation

Condition	Experimental Study	Numerical Study
Fuel density (kg/m^3)	832	780
Air mass flow rate (kg/s)	0.036	0.036
Nozzle diameter (mm)	0.0006	0.0006
Spray half-angle (degree)	31.3	30
Fuel temperature (K)	300	300
Fuel mass flow rate (kg/s)	0.00097	0.00097
Air temperature (K)	300	300
Injection pressure (bar)	7	7

SadatAkhavi et al. [24] recommended a micro gas turbine's combustion characteristic be assessed utilizing liquid fuel in a CAN type combustor. Finding out the chamber's experimental behavior at one of its operating places is the aim of the experimental investigation. A mathematical model is then used to examine the details of the combustion process within the combustor. This combustor has a diameter of 74 mm and a length of 210 mm. Its two rows of six and twelve holes, separated by ten millimeters, are located on its body. A hollow-type pressure swirl injector with a 60° spray angle,

squirts kerosene fuel into the chamber from its central point within the air swirler. Details of the numerical simulation and experimental test are provided in Table 5.

Analyse the combustion chamber's operation. The pattern factor, evaporation efficiency, generated entropy value, and a few other metrics pertaining to combustion in reactive and nonreactive scenarios are measured on the chamber's output plane. The following is the sequence in which the four performance parameters are determined.

$$PF = \frac{T_{max} - T_4}{T_4 - T_3} \tag{8}$$

$$\eta_{combustion} = \frac{C_p(T_{exit} - T_3)\dot{m}_{air}}{\dot{m}_{fuel} LHV fuel} \tag{9}$$

$$\eta_{evaporation} = \frac{\dot{m}_{F \cdot vap}}{\dot{m}_F} \tag{10}$$

$$S_{gen} = \int_{A_{outlet}} \left(\sum_i Y_i s_i\right)(\rho u_j dA_j) + \int_{Walls} \frac{dQ}{T} \tag{11}$$

where, T_{max}, T_4, and T_3 denote the maximum temperature that has been measured, the inlet chamber temperature, and the mean output profile temperature. In addition to the following, T_{exit} calculates the temperature at the chamber exit: discharge, low heat value (LHV), mass flow rate of injected fuel ($\dot{m}_f$), mass flow rate of vaporized fuel $(\dot{m_{f.vap}})$ at the exit, Y_i is the mass fraction, the temperature (T), and the entropy of species i in the mixture (s_i).

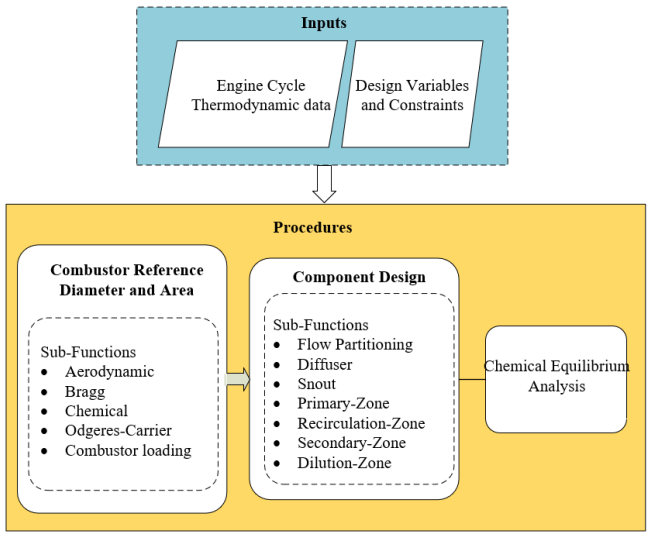

Figure 2. Flow chart of the combustor pre-design tool

Sattelmayer [25] examined the effect of injection pressure and equivalency ratio on combustion in a can combustor. This combustor has two rows of six and twelve holes per 10 mm diameter, measuring 210 mm in length and 74 mm in diameter. Air travels through the primary and intermediate zones via the primary holes and the dilution zone via the secondary holes. Air entering the combustor is directed by an axial 0.86 swirl number swirler downstream of the chamber. The results indicate that when the overall equivalency ratio increases, the combustor temperature increases as well. As the injection pressure is increased while maintaining a steady equivalency ratio, the flame extends downstream to the combustor. Determine the flow field parameters and preliminary geometrical components of the combustor to arrive at the optimal conceptual layout for the component. The flowchart in Figure 2 illustrates the steps.

Zhong et al. [26] suggested the PIV and 2D Mie scattering techniques. Two transparent quartz tubes arranged in a concentric shape constitute the combustion chamber. The outer tube is 100 mm bigger than the inner tube with a diameter of 200 mm. The tubes have an average thickness of 5 mm and a length of 300 mm. The plenum's outer and inner walls measure 290 mm and 202 mm, accordingly. Inside the annulus disk are sixteen equally spaced premixed revolving injectors. The injector features six tangential inlets with a Ds of 3 mm and a Di of 10 mm exit nozzle diameter. Every burner has a small, counter clockwise swirl formed in the injection area. Swirl number S can be analytically found to be approximately 0.8 using Eq. (12).

$$S = \frac{\int_0^R 2\pi\rho v_x v_\theta r^2 dr}{R\int_0^R 2\pi\rho v_x^2 r dr} \tag{12}$$

where, v_x *and* v_θ are in Case 10-357, the injector's axial and azimuthal velocities as determined with an injector outlet are situated about 3 mm above the plane where the Laser Doppler Velocimeter (LDV) is located.

Fu et al. [27] proposed the double-swirler annular combustion chamber of a heavy-duty gas turbine will be subjected to a three-dimensional internal flow and combustion simulation. There are 24 equally distributed dual swirler inlets on the chamber's arc the head face. Set aside 1/24 of the chamber as the computational zone to shorten the computation time. The innermost hole has a length of 0.084 meters and a diameter of 2 R, where R = 0.042 meters. The annulus loop has a diameter of 1.5 R. The combustor's overall length is 30.8 R. 3.4 R is the spherical exit's peak. The subsequent equations that govern can be used to comprehend the turbulent flow, combustion reaction, heat, and mass transport that occur during combustion.

Equation for mass conversion:

$$\frac{\partial \rho}{\partial t} + \frac{\partial}{\partial x_j}(\rho u_j) = 0 \tag{13}$$

Momentum conservation equation:

$$\frac{\partial}{\partial t}(\rho u_i u_j) = -\frac{\partial P}{\partial x_i} + \frac{\partial}{\partial x_j}(T_{ij}) + \rho f_i \tag{14}$$

Energy conservation equation:

$$\frac{\partial}{\partial x_i}(\rho C_P T) + \frac{\partial}{\partial x_i}(\rho C \rho u_j T) = \frac{\partial}{\partial x_j}\left(\frac{\mu}{Pr}\lambda\frac{\partial C_P T}{\partial x_j}\right) + w_s Q_S \tag{15}$$

Composition conservation equation:

$$\frac{\partial}{\partial t}(\rho m_s) + \frac{\partial}{\partial x_j}(p u_j m_s) = \frac{\partial}{\partial x_j}\left(\frac{\mu}{Sc}\frac{\partial m_s}{\partial x_j}\right) - w_s \tag{16}$$

Both the overall temperature of the combustor and the rate at which thermal NOx is produced are lowered by the temperature of the premixed gas at the input. In the situation

that is being considered, the corner recirculation zone has its greatest generation rate (697.24 K) surrounding the combustor's shoulder at 1.9e-06 gmol/(m^3.s).

Sharma et al. [28] developed a can-type gas turbine combustor that uses liquid fuels and operates in flameless combustion mode. Kerosene is used in the combustor, and the 5.1-2.5-2.05 MW/m^3 spectrum of thermally intensities. Air is provided by several injection holes in this novel technique: swirl air close to the fuel injection site, first, second, and dilution air downstream. Across every working parameter sets, the air preheat degree is raised to 950 K to maintain a worldwide uniform ratio. However, for can gas turbine applications, lengthy residence times (~0.5 s) are not desired.

2.4 Swirler effect of gas turbine combustor

A swirler is provided to mix the air and fuel in the combustor. In order to mix fuel and air, the swirler has multiple mixing channels in addition to a number of vanes arranged radially around its central axis. Higher swirl numbers typically result in more intense turbulence and, in turn, faster flames. An overview of a few studies describing the swirler effect of gas turbine combustor is given below.

Zhou et al. [29] suggested a special SSCS was created to increase air performance beneath the squish segments and in the core of the chamber of combustion. For the experimental testing, a single-cylinder diesel engine with model number 1132 Z was employed. The SSCS's power under various spray angle schemes. It is evident that altering the spray angle resulted in the appearance of two peaks. One happened at 116.74 kW with a 165°C A upper spray angle and a 105°C A descending spray angle. With a higher spray angle of 165°C A and a lower spray angle of 75°C A, the other high measured 116.03 kW. A displayed a spray angle of 165°C A upstream and 105°C A downstream, occurring at 116.74 kW. The other peak measured 116.03 kW with a lower spray angle of 75°C A and a higher spray angle of 165°C A. Not every bit of the combustion chamber's air is consumed, and the fuel might not even spread out.

The experiment's conclusions show that the SSCS uses less fuel and produces less soot while using spray angle scheme one. Specifically, fuel consumption fell by 1.6% to 8.3% and soot emissions by 16.16% to 36.64%. Accordingly, 105°C A is the ideal lower spray angle and 165°C A is the ideal higher spray angle in the SSCS. The results of the simulation demonstrate. It is preferred that the fuel/air mixture have less of an impact on the cylinder's initial circumferential ridge in the first spray angle arrangement, which lowers the equivalency proportion. Consequently, angle method for spraying one increases thermal efficiency, produces a more consistent fuel/air combination, and burns less fuel and releases less soot.

Zhou et al. [30] developed a with new separated swirl combustion system (SSCS), the air efficiency in the combustion chamber is intended to be enhanced. Three-dimensional simulation was used to examine the emission characteristics and combustion performance. A sensitivity analysis was conducted on the power output and soot emissions based on different chamber geometries. The experiment part has the following speeds: 1300, 1500, 1800, and 2100 rpm.

Verifying the SSCS engine's performance under various operating circumstances is the goal. The experiment employed a single-cylinder, 132 mm-diameter diesel engines. For gasoline supply, a Bosch electronic unit pump was employed. The plunger had a diameter of 12 mm and a pre-stroke of 9 mm. The AC electrical dynamometer utilized for the test has a speed accuracy of ± 2 r/min, torque precision of ± 0.2% FS, a maximum absorption power of 160 kW also a maximum speed of 4500 r/min. Despite the fact that the SSCS and DSCS emitted more NOx at different speeds. As indicated in Table 6, the simulation model was configured in accordance with the rated experimental parameters.

Table 6. Experimental parameter for combustion chamber

Parameter	Values
Exhaust valve opening time	460°C A
Stroke	145 mm
Initial temperature	401.3 K
Connecting rod length	262 mm
Speed	2500 r/min
Cylinder diameter	132 mm
Compression ratio	13.5
Injection timing	348°C A
Injection quantity	36 mg
Nozzle diameter	0.27 mm
Initial pressure	5.26 bar
Intake valve closing time	239.5°C A

Both of the test's combustion systems had eight nozzles, 210 bar of needle valve opening pressure, and 0.27 mm injector diameters. A double swirl combustion system (DSCS) has a nozzle angle of 145 degrees. At various machine speeds, comparisons demonstrate that the SSCS exhibits lower brake-specific fuel consumption (BSFC) also higher indicated thermal efficiency than the DSCS. At 2100 r/min, the SSCS notably reduced fuel consumption by approximately 6.54 g/(kW h) and lowered soot emissions by 2.89% to 0.17 FSN.

After-treatment methods can reduce NOx emission, even if it is higher and occur different speeds in the SSCS and DSCS. Given that the DSCS's performance has been tested before, The SSCS (Single Shaft Combined Cycle System) finds broad application thanks to its superior emission in addition to combustion performance across a wide range of operating speeds. The DSCS was also used to confirm the SSCS results.

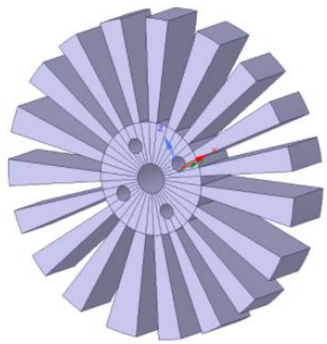

Figure 3. Schematic representation of swirler

Belal et al. [31] suggested a quantitative comparison based on testing, represents two swirl burners with two separate designs and the same swirl number (0.55), in addition to the hot conditions of combustion and emission and the turbulent field of flow (cold flow). With its annular outer swirler (swirl angle of 40) and numerous core circular jets, the first burner generates "small swirl ignition." The second burner, in contrast, generates "high swirl ignition" due to its central recirculation zone, outer swirler with a 35 degree of swirl

angle, and obstructed central passage. Both burner designs exhibit different aerodynamic flow patterns but share the identical symmetrical swirl number (SN = 0.55). It was unclear what the reacting flow's findings were. The gas turbine combustion swirler is shown in Figure 3.

A vertical, uncooled cylindrical steel pipe, measuring 0.5 meters in length, with an inner diameter of 0.15 meters and a wall thickness of 3 millimeters, is used in the setup. To facilitate axial and radial point measurements, a 1-centimeter-wide longitudinal slit has been machined along the pipe's surface.

Air is supplied by a screw compressor connected to a 2 m^3 capacity storage tank. The preparation section consists of a 1-meter-long insulated pipe with an inner diameter of 45 millimeters. The fuel injector is positioned at the inlet of this section, while the burner is located at the outlet.

The initial burner design employs a Low Swirl Combustor (LSC) configuration, incorporating perforated core piping and an outer swirler with a high swirl angle of 40 degrees.

The second burner, an HSC (High Swirl Combustor), has a swirl angle of 35 degrees and includes a fully enclosed core configuration. Additionally, an external coaxial vane swirler is incorporated. Consequently, the generated flames feature the distinctive core circulation region. The method for calculating of the LSC burner's swirl number is given by Eq. (17). The mathematical representation of the swirl number (m ¼ 0) for the HSC burner can be obtained from Eq. (18).

$$SN = \frac{2}{3}\tan\theta \frac{1 - R^3}{1 - R^2 + m^2\left(\left({}^{1}/_{R^2}\right) - 1\right)^2 R^2} \tag{17}$$

$$SN = \frac{2}{3}\left[\frac{1 - \left(\frac{R_c}{R_b}\right)^3}{1 - \left(\frac{R_c}{R_b}\right)^2}\right] tan\theta \tag{18}$$

where, R is equal to $\left(\frac{R_c}{R_b}\right)$, where R_b is the swirler outer radius and R_c is the core channel radius. The mass split ratio is m = m_c/m_s, where m_c is the center's mass flux and m_s is the swirled outer flow's mass flux. θ is the swirl angle of the outer swirler.

Chiong et al. [32] examined the burning properties of a mixture utilizing a model gas turbine swirl burner at vane angles (θ) of 30°, 45°, and 60° of natural gas (NG) and palm biodiesel/methyl esters (PME). Liquid fuel was atomized at an air-to-liquid ratio (ALR) of 2.50% using a dual fluid air blast atomizer. An axial swirler was used to start the swirling flow while the main air flowed through it. At the burner output, a combustible combination was created when the liquid fuel spray and whirling air flow combined. An axial swirler with six straight vanes, concentrically positioned near the burner exit, created swirl at vane angles (θ) of 30, 45, and 60 degrees, resulting in low, medium, and extensive swirl, respectively. Eq. (19), where D_h, D_s and θ stand for the vane angle, swirler hub diameter, and swirler diameter, correspondingly, was used to calculate the swirler's dimensions and the swirl number. The values of the swirl numbers for θ = 30°, 45°, and 60° are 1.12, 0.56, and 0.84, in that order.

$$S_N = \frac{2}{3}\left[\frac{1 - (D_h/D_s)^3}{1 - (D_h/D_s)^2}\right] tan\theta \tag{19}$$

Eqs. (20) and (21) were used to determine the mass average chain length (CL) and degree of unsaturation (DOU) of the PME were determined to be 17.2 and 0.622, respectively.

$$CL = \frac{\sum_{i=1}^{n}(n_i C_i)}{100} \tag{20}$$

$$DOU = \frac{\sum_{i=1}^{n}(n_i B_i)}{100} \tag{21}$$

The fatty acid i's mass proportions are represented by the word n, whilst the term C specifies how many carbons it contains. The number of double bonds is represented by the letter B. A modest flame liftoff is the main feature of the PME/NG swirl flame. Inhibiting axial flame growth, a high vane angle of sixty degrees intensifies the vortical flow and directs the flame in a radial direction. However, for the θ = 30° operation, flame liftoff does not occur. This leads to a narrower luminous reaction zone than for θ = 45° and 3 0. Large dissipation rates yield much lower radical intensities when burning at θ = 60° compared to θ = 45° and 30°. Furthermore, because of the significant drop in thermal NO, NO emissions for PME and PME/NG combustion are significantly reduced while running at vane angles of θ = 60°.

Patel and Shah [33] examine the impact of swirl and the number of vanes on the combustion characteristics of the methane inverse diffusion flame (IDF). The structure and appearance of IDFs are examined in relation to the effects of changing the number of vanes (4, 6, and 8). Dual flame structures appear in swirling IDFs. The diameter ratio of the burner's concentric tubes is 1.95. An outer tube with a diameter of 37 mm and an inner tube with a diameter of 19 mm make up the coaxial burner. With fuel and air delivered independently. A blower is used to supply air. The fuel is delivered by a methane cylinder. A calibrated mass flow controller is used to measure the fuel flow rate. A calibrated thermal mass flow meter is used to monitor the airflow rate. The definition of equivalency ratio, ϕ in Eq. (22).

$$\phi = (M_a/M_f)_{stoich} \,/\, ((M_a/M_f)_{actual}) \tag{22}$$

Using a fixed swirler vane angle of 30°, the study investigates how varying the number of swirler shafts (four, six, and eight) affects the structure and appearance of the flame. The fuel flow rate varies during the experiments from 2.8 to 8.0 lpm whereas the air flow rate is fixed at 125 lpm (Reair = 9454). Consequently, to get from 0.2 to 0.6, Φ rises by 0.1. Below Z = 140 mm, the temperature gradient along the centerline of the IDF in swirl is more pronounced compared to that of the IDF without swirl. IDF's temperature steadily rises until it surpasses 1190 K (Z = 145 mm), at which point it stops swirling and starts to fall. IDF in swirl, degree rises sharply to 1632K at Z=60mm, followed by a gradual decrease thereafter.

The IDFs with six vane spirals produce the least NOx. However, non-swirling, weakly premixed IDFs were visible in the inner reaction zone.

Vigueras-Zúñiga et al. [34] suggested the combined cycle (CC) biogas combustion experimental testing and numerical modeling based on computational fluid dynamics (CFD), with a 2.48 swirl number (Sn) from an improved swirler in the airstream. Turbulence swirl values range from 0.6 to 2.5. The turbulence was analyzed using a turbulence model called the renormalization group (RNG). The numerical model enables visualization of the recirculation zone formed by the intense swirl in the primary and partially of the intermediate zones in

the combustion chamber. A strong airstream swirl in the center of the CC creates low-velocity zones. Positioning the flame in the center prevents localized hot spots around the flame tube and reduces the risk of flashback occurring at structural components. Covering a sizable portion of the flame tube; nonetheless, the temperatures are lower.

Xu et al. [35] analyzed the combustion instabilities in a premixed swirl combustor through both theoretical and experimental methods. The swirler is the source of the flow disturbance that alters the flame reaction in addition to producing swirling flow. There is an axial swirler with a swirl number of approximately 0.6 and a bluff body within the 20 mm-diameter mixing channel. Modulating the swirl position changes results in variations in the time delay and gain. The flame tube has a consistent distribution of velocity, with the exception of the fuel injection point, where the maximum velocity of 20.29 m/s is recorded. Covering a sizable portion of the flame tube, nevertheless the temperatures are not as high.

Gas turbine combustors face several limitations across different design aspects. The use of various fuels introduces challenges such as inconsistent combustion properties, corrosion, deposit formation, and high NOx emissions, which are difficult to manage with traditional combustor designs. Temperature variation within the combustor leads to thermal stresses, material degradation, and combustion instability, particularly at high operating temperatures. Different combustor shapes present trade-offs between compactness, ease of maintenance, and uniformity of temperature distribution, often complicating performance optimization. Additionally, swirlers, which are used to enhance mixing and flame stability, can cause pressure losses and combustion instabilities if not properly designed. In the future, these issues can be mitigated through the development of fuel-flexible combustors, advanced cooling techniques, smart materials, adaptive combustion control using AI, and optimized geometries guided by high-fidelity simulations and additive manufacturing technologies.

3. RESULT AND DISCUSSION

A combustor, or burner, is a component of gas turbine engines where high-pressure air is mixed with fuel and burned. When the exhaust gas is directed via a nozzle, it produces thrust and turns the power turbine due to its high temperature. Additionally, ramjet and scramjet propulsion systems employ burners. This paper analyzes four performance-driven approaches for gas turbine combustor: different kind of fuels, combustor shapes, varying the swirl and different temperatures. The graphical representation of these comparisons is shown below. The testing setup included an Nvidia GeForce, GTX 1650 graphics card, an Intel Core i5 processor, 16GB of RAM, and Python 3.8.

3.1 Performance of the gas turbine combustor for various fuel types

In this section various fuel types of gas turbine combustor performance are compared. Fuel mass flow rate (kg/s) and inlet temperature (K) are the performance utilized for the comparison.

Figure 4 presents a comparison of the fuel mass flow rates reported in various studies on gas turbine combustors. In this study, Kahraman et al. [11] achieved a fuel mass flow rate of 0.069 kg/s, the highest among the reviewed works. For comparison, Liu et al. [12] reported 0.014 kg/s, Wang et al. [13] reported 0.002 kg/s, Ajvad and Shih [14] reported 0.010 kg/s, and Chen et al. [15] reported 0.034 kg/s.

Figure 5 compares the inlet temperatures used in the gas turbine combustors. Kahraman et al. [11] achieved the highest inlet temperature at 350 K, while the other studies—Liu et al. [12], Wang et al. [13], Ajvad and Shih [14], and Chen et al. [15]—reported an inlet temperature of 172 K.

The observed variations in fuel mass flow rates and inlet temperatures across these studies can be attributed to differences in combustor design objectives, fuel types, and operating conditions.

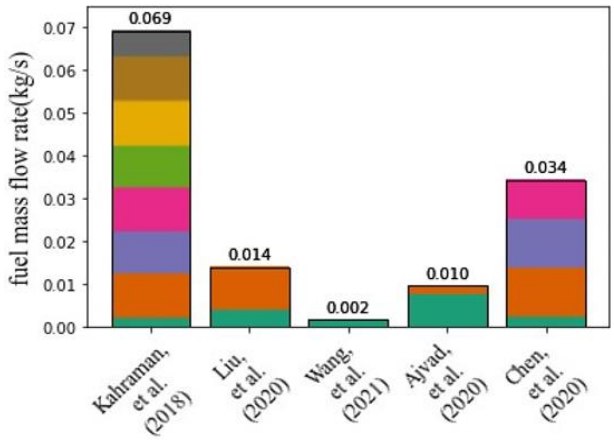

Figure 4. Comparison of fuel mass flow rate (kg/s)

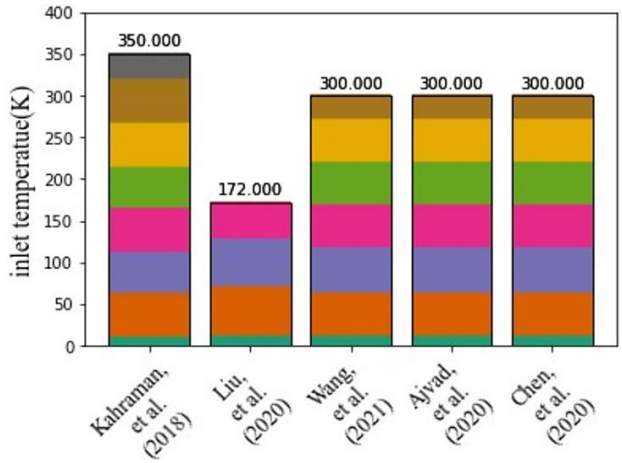

Figure 5. Comparison of inlet temperature (K)

3.2 Performance of the gas turbine combustor for various temperature

The performance of gas turbine combustor at different temperatures is compared in this section. Pressure (bar) and wall temperature (K) are the performance metrics utilized in this comparison.

Figure 6 presents a comparison of the wall temperatures of gas turbine combustors reported in various studies. The following values were recorded: 580 K by Singh et al. [17], 1000 K by Schulz and Noiray [18], 750 K by Somarathne et al. [19], 1400 K by Nau et al. [20], and 873 K by Mekhrengin et al. [21].

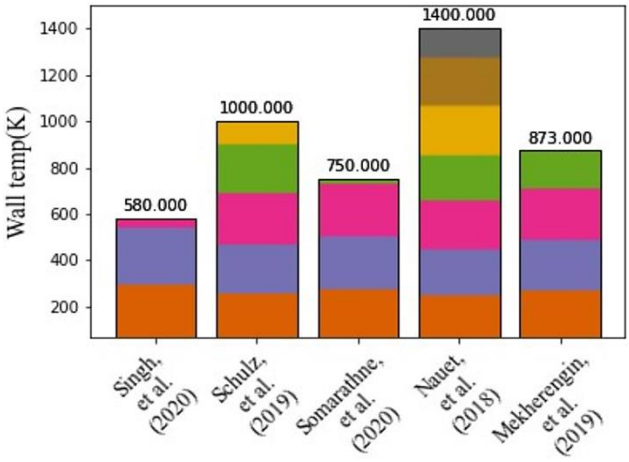

Figure 6. Comparison of wall temperature (K)

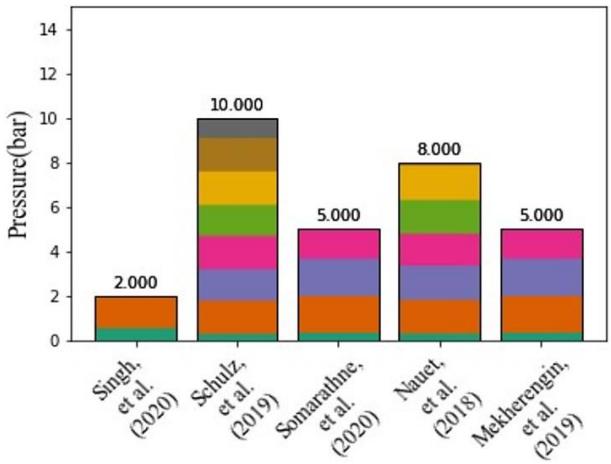

Figure 7. Comparison of pressure (bar)

Figure 7 compares the combustor operating pressures (in bar) reported in the same studies. The recorded pressures are: 2 bar by Singh et al. [17], 10 bar by Schulz and Noiray [18], 5 bar by Somarathne et al. [19], 8 bar by Nau et al. [20], and 5 bar by Mekhrengin et al. [21]. Among these, Schulz and Noiray [18] achieved the highest operating pressure.

The observed differences in wall temperature and operating pressure across the studies are likely due to variations in combustor design, material properties, cooling strategies, and operating conditions.

3.3 Performance of the gas turbine combustor for different combustor shape

The efficiency of gas turbine fuel for different combustion pattern is compared in this section. Axial velocity (m/s) and temperature (K) are the performance metrics that are used in this comparison.

Figure 8 presents a comparison of the axial velocities in various gas turbine combustor studies. The reported axial velocities are as follows: 18 m/s by Zettervall et al. [23], 40.58 m/s by SadatAkhavi et al. [24], 15.953 m/s by Sattelmayer [25], 3 m/s by Zhong et al. [26], and 30 m/s by Fu et al. [27]. Among these, SadatAkhavi et al. [24] achieved the highest axial velocity.

Figure 9 illustrates a comparison of the combustor temperatures across different gas turbine combustor models. The following temperatures were reported: 2212 K by Zettervall et al. [23], 817.97 K by SadatAkhavi et al. [24], 1650 K by Sattelmayer [25], 1783 K by Zhong et al. [26], and 600 K by Fu et al. [27]. The highest temperature was achieved by Zettervall et al. [23].

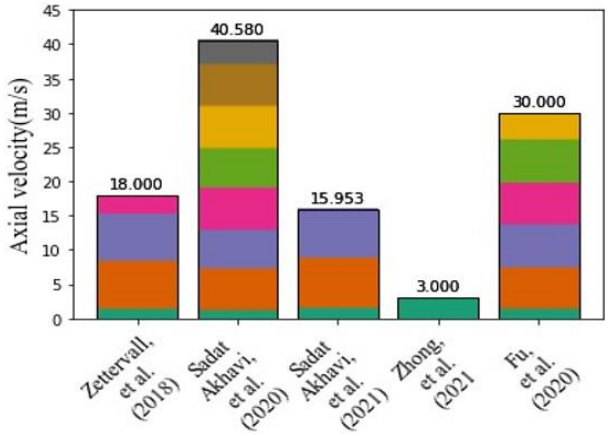

Figure 8. Comparison of axial velocity (m/s)

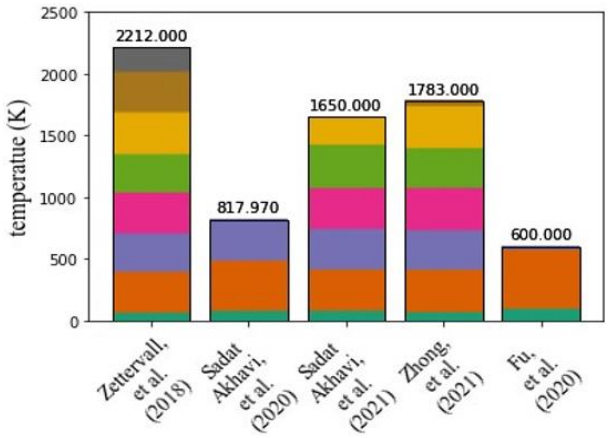

Figure 9. Comparison of temperature (K)

The differences observed across the studies highlight the significant influence of combustor geometry, fuel-air mixing efficiency, and operating conditions on flow dynamics and thermal behavior.

3.4 Performance of the gas turbine combustor for effect of swirl

The performance of the gas turbine combustor in the effect of swirl is compared in this section. Temperature (K) and pressure (bar) are the performance metrics that are used in this comparison.

Figure 10 presents a comparative analysis of the combustor temperatures in various gas turbine studies. The following results were reported: 401.3 K by Zhou et al. [29], 401.3 K by Zhou et al. [30], 523 K by Belal et al. [31], 523 K by Chiong et al. [32], and 900 K by Patel and Shah [33]. Among these, Patel and Shah [33] achieved the highest temperature.

Figure 11 compares the combustor pressures (in bar) across the same studies. The reported values are: 5.26 bar by Zhou et al. [29], 5.26 bar by Zhou et al. [30], 4.8 bar by Belal et al. [31], 6.1 bar by Chiong et al. [32], and 6.3 bar by Patel and Shah [33]. Again, Patel and Shah [33] attained the highest pressure among the reviewed publications.

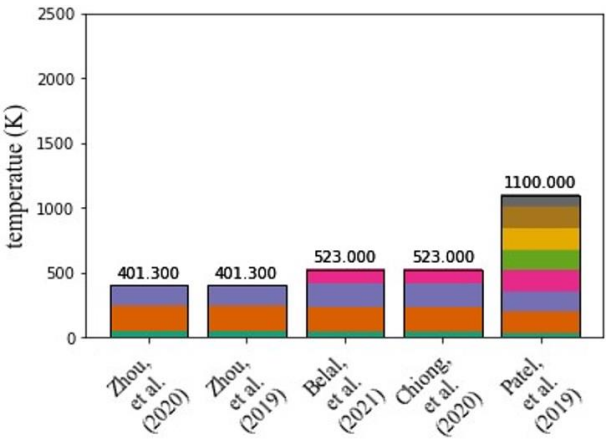

Figure 10. Comparison of temperature (K)

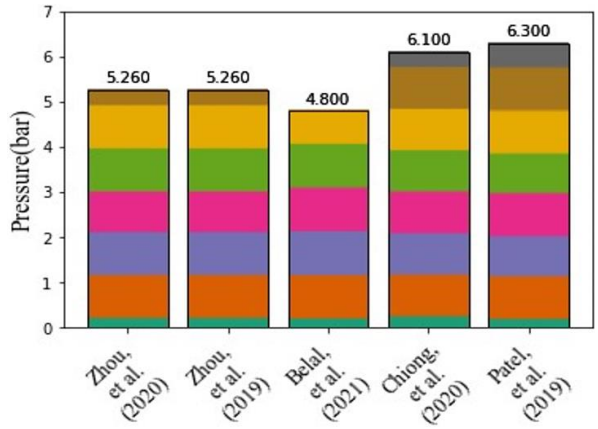

Figure 11. Comparison of pressure (bar)

These results suggest that the combustor configuration used by Patel and Shah [33] may have been optimized for high energy release and efficient combustion, potentially through the use of a richer fuel-air mixture or operation at higher mass flow rates.

3.5 Suggestions

Recent years have seen significant advancements in the design of contemporary gas turbines, as well as in the use of alternate fuels, temperature, swirler effect, and combustion shapes. To offer a more varied energy source and lessen the impact on environmental pollutants, which may offer direction for the development and evaluation of the viability of gas turbine combustor technology. Various conditions such as different fuels, combustor shapes, swirl effects and temperatures are considered for designing the gas turbine combustor for this comparative paper. Hydrogen fuel is best option for combustion process, when compared with other type of fuels such as, methane, syngas, biogas and propane. Among various temperature conditions, at 1400 K temperature, the gas turbine performs better. Can shape combustor is the best design among different types of combustor shapes. At last, swirler angle of 30 degree is best suitable for inverse diffusion flame.

4. CONCLUSION

Gas turbines are extensively utilized equipment for power generation globally. The three primary components of a gas turbine are the compressor, combustor, and turbine. The gas turbine combustor's operational window is incredibly narrow. Lean-premixed turbulent combustion is made easier with the help of the combustor, which lowers NOx emissions. Lean-premixed turbulent combustion has low emissions, but because of pressure dynamics, the flame is highly unstable. A high-pressure working fluid is created from the air as it passes through the compressor and the air intake system. Power is produced via its reaction with fuel in the combustor, expansion in the turbine, and operation of the generator. The paper examines the gas turbine combustor using many different kinds of fuel types, temperatures, combustor shapes, and swirl effects. Analysed gas turbine combustor performance with different fuels, such as methane, hydrogen, syngas, biogas, and propane. When compared to other fuel types, hydrogen fuel has the highest fuel mass flow rate and inlet temperature of 0.069 kg/s and 350 K. Values of temperature at the combustion chamber output was 3–10%. Then the gas turbine combustor performance was evaluated with different temperatures conditions. At 1700 K, a high wall temperature of 1400 K was achieved when compared to other temperature conditions. A broad range of points especially at 10 bars, because the laminar flame speed is more variable than the atmospheric pressure flame. The performance of the gas turbine combustor was assessed under different combustor shapes. Maximum Axial velocity of 40.58 m/s was obtained in MICCA-type annular combustor. Finally, the gas turbine combustor performance was evaluated with various swirler effects. A maximum pressure and temperature like 6.3 bar and 1100 K were obtained at 90° of swirler angle when compared to others.

Compared to baseline CI mode combustion, the various techniques used for comparison in this research have a number of shortcomings, including uncontrolled combustion, banging at high engine loads, and combustion that emits relatively less NOx. So, different mechanisms and scenarios by varying the casting angle and dump gap between the swirler and linear in the gas turbine combustor will develop in the future which might lead to random dynamic pressure and heat release rate bursts.

REFERENCES

[1] Stefanizzi, M., Capurso, T., Filomeno, G., Torresi, M., Pascazio, G. (2021). Recent combustion strategies in gas turbines for propulsion and power generation toward a zero-emissions future: Fuels, burners, and combustion techniques. Energies, 14(20): 6694. https://doi.org/10.3390/en14206694

[2] Okafor, E.C., Somarathne, K.K.A., Ratthanan, R., Hayakawa, A., Kudo, T., Kurata, O., Kobayashi, H. (2020). Control of NOx and other emissions in micro gas turbine combustors fuelled with mixtures of methane and ammonia. Combustion and Flame, 211: 406-416. https://doi.org/10.1016/j.combustflame.2019.10.012

[3] Lada, E.K., Steiger, N.M., Wilson, J.R. (2006). Performance evaluation of recent procedures for steady-state simulation analysis. IIE Transactions, 38(9): 711-727. https://doi.org/10.1080/07408170600735520

[4] Silva, F.C.N., Flórez-Orrego, D., de Oliveira Junior, S. (2019). Exergy assessment and energy integration of advanced gas turbine cycles on an offshore petroleum production platform. Energy Conversion and

Management, 197: 111846. https://doi.org/10.1016/j.enconman.2019.111846
[5] Kabeyi, M.J.B., Olanrewaju, O.A. (2022). Geothermal wellhead technology power plants in grid electricity generation: A review. Energy Strategy Reviews, 39: 100735. https://doi.org/10.1016/j.esr.2021.100735
[6] Roy, D., Samanta, S., Ghosh, S. (2019). Techno-economic and environmental analyses of a biomass based system employing solid oxide fuel cell, externally fired gas turbine and organic Rankine cycle. Journal of Cleaner Production, 225: 36-57. https://doi.org/10.1016/j.jclepro.2019.03.261
[7] Mikielewicz, D., Kosowski, K., Tucki, K., Piwowarski, M., Stępień, R., Orynycz, O., Włodarski, W. (2019). Gas turbine cycle with external combustion chamber for prosumer and distributed energy systems. Energies, 12(18): 3501. https://doi.org/10.3390/en12183501
[8] Cecere, D., Giacomazzi, E., Di Nardo, A., Calchetti, G. (2023). Gas turbine combustion technologies for hydrogen blends. Energies, 16(19): 6829. https://doi.org/10.3390/en16196829
[9] Sathish, T., Jayarajeswaran, R., Karthick, S. (2018). Finite element analysis of the stress and strain patterns in pyramidal hopper. International Journal of Rapid Manufacturing, 7(4): 374-387. https://doi.org/10.1504/IJRAPIDM.2018.095810
[10] Chen, Z.X., Langella, I., Swaminathan, N., Stöhr, M., Meier, W., Kolla, H. (2019). Large Eddy Simulation of a dual swirl gas turbine combustor: Flame/flow structures and stabilisation under thermoacoustically stable and unstable conditions. Combustion and Flame, 203: 279-300. https://doi.org/10.1016/j.combustflame.2019.02.013
[11] Kahraman, N., Tangöz, S., Akansu, S.O. (2018). Numerical analysis of a gas turbine combustor fueled by hydrogen in comparison with jet-A fuel. Fuel, 217: 66-77. https://doi.org/10.1016/j.fuel.2017.12.071
[12] Liu, A., Yang, Y., Chen, L., Zeng, W., Wang, C. (2020). Experimental study of biogas combustion and emissions for a micro gas turbine. Fuel, 267: 117312.
[13] Wang, J., Hu, Z., Du, C., Tian, L., Baleta, J. (2021). Numerical study of effusion cooling of a gas turbine combustor liner. Fuel, 294: 120578. https://doi.org/10.1016/j.fuel.2021.120578
[14] Ajvad, M., Shih, H.Y. (2020). Modeling syngas combustion performance of a can combustor with rotating casing for an innovative micro gas turbine. International Journal of Hydrogen Energy, 45(55): 31188-31201. https://doi.org/10.1016/j.ijhydene.2020.08.113
[15] Chen, J., Song, W., Xu, D. (2017). Optimal combustor dimensions for the catalytic combustion of methane-air mixtures in micro-channels. Energy Conversion and Management, 134: 197-207. https://doi.org/10.1016/j.enconman.2016.12.028
[16] Bonasio, V., Ravelli, S. (2022). Performance analysis of an ammonia-fueled micro gas turbine. Energies, 15(11): 3874. https://doi.org/10.3390/en15113874
[17] Singh, A.P., Kumar, V., Agarwal, A.K. (2020). Evaluation of comparative engine combustion, performance and emission characteristics of low temperature combustion (PCCI and RCCI) modes. Applied Energy, 278: 115644. https://doi.org/10.1016/j.apenergy.2020.115644
[18] Schulz, O., Noiray, N. (2019). Combustion regimes in sequential combustors: Flame propagation and autoignition at elevated temperature and pressure. Combustion and Flame, 205: 253-268. https://doi.org/10.1016/j.combustflame.2019.03.014
[19] Somarathne, K.D.K.A., Okafor, E.C., Sugawara, D., Hayakawa, A., Kobayashi, H. (2021). Effects of OH concentration and temperature on NO emission characteristics of turbulent non-premixed CH_4/NH_3/air flames in a two-stage gas turbine like combustor at high pressure. Proceedings of the Combustion Institute, 38(4): 5163-5170. https://doi.org/10.1016/j.proci.2020.06.276
[20] Nau, P., Yin, Z., Lammel, O., Meier, W. (2019). Wall temperature measurements in gas turbine combustors with thermographic phosphors. Journal of Engineering for Gas Turbines and Power, 141(4): 041021. https://doi.org/10.1115/1.4040716
[21] Mekhrengin, M.V., Meshkovskii, I.K., Tashkinov, V.A., Guryev, V.I., Sukhinets, A.V., Smirnov, D.S. (2019). Multispectral pyrometer for high temperature measurements inside combustion chamber of gas turbine engines. Measurement, 139: 355-360. https://doi.org/10.1016/j.measurement.2019.02.084
[22] Chen, F., Ruan, C., Yu, T., Cai, W., Mao, Y., Lu, X. (2019). Effects of fuel variation and inlet air temperature on combustion stability in a gas turbine model combustor. Aerospace Science and Technology, 92: 126-138. https://doi.org/10.1016/j.ast.2019.05.052
[23] Zettervall, N., Worth, N.A., Mazur, M., Dawson, J.R., Fureby, C. (2019). Large eddy simulation of CH4-air and C2H4-air combustion in a model annular gas turbine combustor. Proceedings of the Combustion Institute, 37(4): 5223-5231. https://doi.org/10.1016/j.proci.2018.06.021
[24] SadatAkhavi, S., Tabejamaat, S., EiddiAttarZade, M., Kankashvar, B. (2020). Experimental and numerical study of combustion characteristics in a liquid fuel CAN micro-combustor. Aerospace Science and Technology, 105: 106023. https://doi.org/10.1016/j.ast.2020.106023
[25] Sattelmayer, T. (2003). Influence of the combustor aerodynamics on combustion instabilities from equivalence ratio fluctuations. Journal of Engineering for Gas Turbines and Power, 125(1): 11-19. https://doi.org/10.1115/1.1365159
[26] Zhong, L., Yang, Y., Jin, T., Xia, Y., Fang, Y., Zheng, Y., Wang, G. (2021). Local flame and flow properties of propagating premixed turbulent flames during light-round process in a MICCA-type annular combustor. Combustion and Flame, 231: 111494. https://doi.org/10.1016/j.combustflame.2021.111494
[27] Fu, Z., Gao, H., Zeng, Z., Liu, J., Zhu, Q. (2020). Generation characteristics of thermal NOx in a double-swirler annular combustor under various inlet conditions. Energy, 200: 117487. https://doi.org/10.1016/j.energy.2020.117487
[28] Sharma, S., Chowdhury, A., Kumar, S. (2020). A novel air injection scheme to achieve MILD combustion in a can-type gas turbine combustor. Energy, 194: 116819.
[29] Zhou, H., Li, X., Chen, Y., Kang, Y., Liu, D., Liu, F. (2020). The effect of spray angle on the combustion and emission performance of a separated swirl combustion system in a diesel engine. Energy, 190: 116481. https://doi.org/10.1016/j.energy.2019.116819
[30] Zhou, H., Li, X., Zhao, W., Liu, F. (2019). Effects of

separated swirl combustion chamber geometries on the combustion and emission characteristics of DI diesel engines. Fuel, 253: 488-500. https://doi.org/10.1016/j.fuel.2019.05.032

[31] Belal, B.Y., Li, G., Zhang, Z., El-Batsh, H.M., Moneib, H.A., Attia, A.M.A. (2021). The effect of swirl burner design configuration on combustion and emission characteristics of lean pre-vaporized premixed flames. Energy, 228: 120622. https://doi.org/10.1016/j.energy.2021.120622

[32] Chiong, M.C., Valera-Medina, A., Chong, W.W.F., Chong, C.T., Mong, G.R., Jaafar, M.N.M. (2020). Effects of swirler vane angle on palm biodiesel/natural gas combustion in swirl-stabilised gas turbine combustor. Fuel, 277: 118213. https://doi.org/10.1016/j.fuel.2020.118213

[33] Patel, V., Shah, R. (2019). Effect of swirl and number of swirler vanes on combustion characteristics of methane inverse diffusion flame. Journal of Mechanical Science and Technology, 33: 1947-1958. https://doi.org/10.1007/s12206-019-0345-7

[34] Vigueras-Zúñiga, M.O., Ramírez-Ruíz, C.A., Herrera-May, A.L., Tejeda-del-Cueto, M.E. (2021). Numerical and experimental analysis of the effect of a swirler with a high swirl number in a biogas combustor. Energies, 14(10): 2768. https://doi.org/10.3390/en14102768

[35] Xu, L., Zheng, J., Wang, G., Li, L., Qi, F. (2022). Effects of swirler position on flame response and combustion instabilities. Chinese Journal of Aeronautics, 35(3): 345-355. https://doi.org/10.1016/j.cja.2021.07.036